

Supplementary information for

Improving thermoelectric performance of indium thiospinel by Se- and Te-substitution

Paweł Wyżga^{1,2}, Sven Grimm¹, Valentin Garbe³, Esteban Zuñiga-Puelles^{1,2}, Cameliu Himcinschi⁴, Igor Veremchuk^{2,5}, Andreas Leithe-Jasper², Roman Gumeniuk¹

¹ Institut für Experimentelle Physik, TU Bergakademie Freiberg, Leipziger Str. 23, 09599 Freiberg, Germany

² Max-Planck-Institut für Chemische Physik fester Stoffe, Nöthnitzer Straße 40, 01187 Dresden, Germany

³ Institut für Angewandte Physik, TU Bergakademie Freiberg, Leipziger Str. 23, 09599 Freiberg, Germany

⁴ Institut für Theoretische Physik, TU Bergakademie Freiberg, Leipziger Str. 23, 09599 Freiberg, Germany

⁵ Institute for Ion Beam Physics and Materials Research, Helmholtz-Zentrum Dresden-Rossendorf, Bautzner Landstraße 400, 01328 Dresden, Germany

1. Powder X-ray diffraction

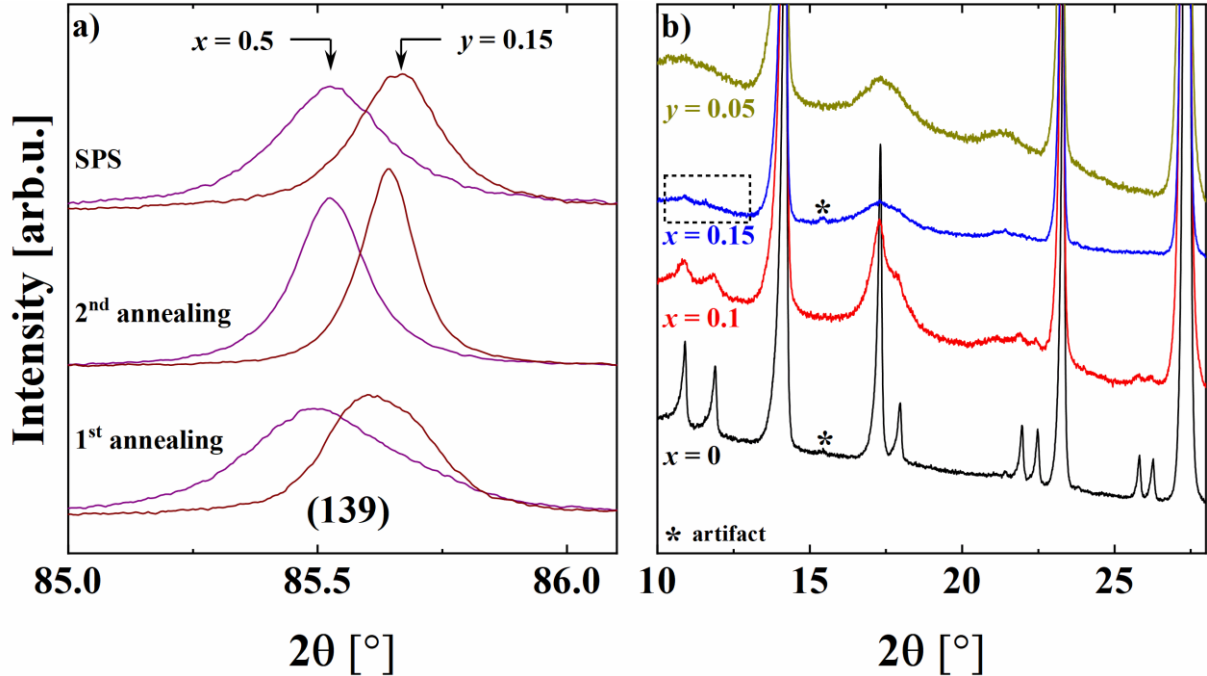


Figure S1. a) PXRD reflection (139) of $\text{In}_{2.67}\text{S}_{3.5}\text{Se}_{0.5}$ and $\text{In}_{2.67}\text{S}_{3.85}\text{Te}_{0.15}$ after synthesis and SPS fabrication. A broadening of PXRD peaks after SPS can be ascribed to the reduced grain size (samples were ground before SPS). b) Disappearing of tetragonal superstructural reflections upon Se/Te-incorporation in $\text{In}_{2.67}\text{S}_{4-x}\text{Se}_x$ and $\text{In}_{2.67}\text{S}_{4-y}\text{Te}_y$ compounds. Bumps at 17.5 and 22° originate from the thin film of vaseline used to fix powders on the sample holder.

Powder X-ray diffraction analysis after the 1st annealing step revealed the formation of at least two thiospinel phases with close chemical compositions and similar unit-cell parameters (significant peak asymmetry and increased full-width at half-maximum of reflections at high 2θ -angles, Figure S1a).

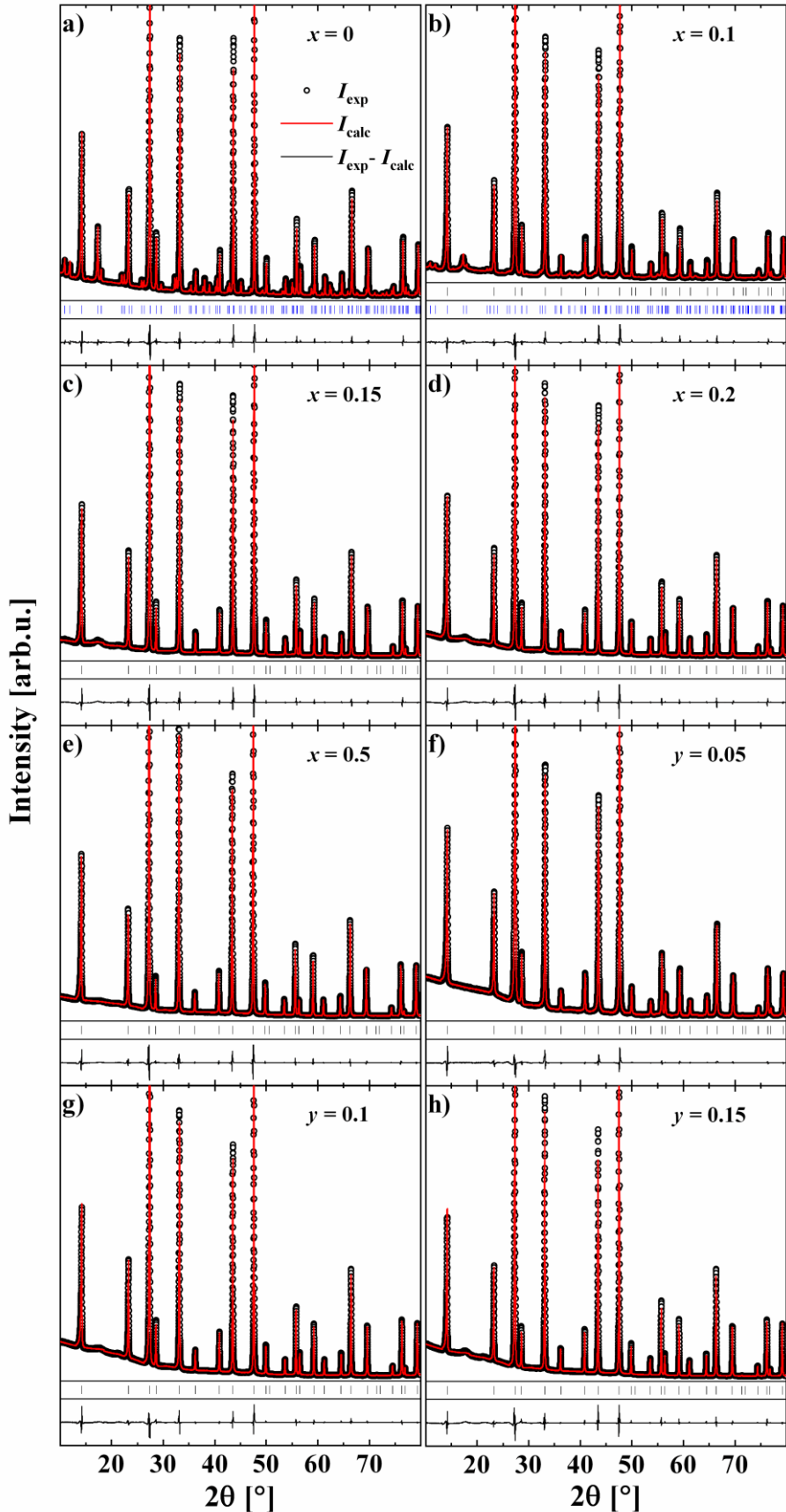


Figure S2. Experimental, refined and differential PXRD profiles of $\text{In}_{2.67}\text{S}_{4-x}\text{Se}_x$ (a–e) and $\text{In}_{2.67}\text{S}_{4-y}\text{Te}_y$ (f–h) samples from Rietveld refinement. Intensities in patterns were normalized according to the most intense reflection.

Table S1. Crystallographic parameters from Rietveld refinement of Se- and Te-substituted samples using the tetragonal *I4₁/amd* structural model.

Nominal composition x	In _{2.67} S _{4-x} Se _x	
	0	0.1
Type of refinement	single-phase	two-phase
Space group, Pearson symbol, no. of formula units Z		<i>I4₁/amd</i> , <i>tI80</i> , 16
a [Å] ^{a)}	7.61891(7)	7.6274(3)
c [Å] ^{a)}	32.3245(5)	32.360(1)
V [Å ³] ^{a)}	1876.4(1)	1882.6(1)
d_{XRD} [g·cm ⁻³] ^{b)}	4.6137(3)	4.6480(3)
λ [Å]		1.54056
$2\theta_{\text{max}}$ [°], $\sin\theta/\lambda$ (max)		100.30; 0.498
No. of refined reflections		296
R_I , $R_{P,\text{CSD}}$, $R_{WP,\text{CSD}}$ [%]	5.25, 11.27, 11.22	16.44, 14.08, 14.84
R_P , R_{WP} [%]	4.16, 6.35	5.51, 7.97
Phase fraction [%]	-	31
In1 at $8c$ (0 0 0) / B_{iso} [Å ²]	1.7(3)	1.7(3)
In2 at $16h$ (0 y z) / B_{iso} [Å ²]	-0.0186(8), 0.3328(4) / 1.30(15)	-0.016(3), 0.3328(10) / 1.38(3)
In3 at $8e$ (0 $1/4$ z) / B_{iso} [Å ²]	0.2043(4) / 1.2(1)	0.204(11) / 1.20(3)
S1 at $16h$ (0 y z) / B_{iso} [Å ²]	-0.013(4), 0.247(1) / 1.0(8)	-0.02(1), 0.247(3) / 0.97(3)
S2 at $16h$ (0 y z) / B_{iso} [Å ²]	0.009(4), 0.082(2) / 1.3(6)	0.012(9), 0.081(4) / 1.33(3)
S3 at $16h$ (0 y z) / B_{iso} [Å ²]	0.027(4), 0.416(1) / 1.1(6)	0.033(9), 0.416(4) / 1.10(3)
$4 \times \text{In1-S1}, 2 \times \text{In1-S2}$ [Å]	2.62(2), 2.66(5)	-
$1 \times \text{In2-S1}, 2 \times \text{In2-S2}, 1 \times \text{In2-S3},$ $2 \times \text{In2-S3}$ [Å]	2.76(4), 2.54(2), 2.70(5), 2.66(2)	-
$2 \times \text{In3-S1}, 2 \times \text{In3-S3}$ [Å]	2.44(4), 2.45(3)	-

a) Given unit-cell parameters were refined separately with LaB₆ as an internal standard (values are also shown in the Figure 2).

b) Densities were calculated for nominal chemical compositions.

Table S2. Crystallographic parameters from Rietveld refinement of Se- and Te-substituted samples using the cubic $Fd\bar{3}m$ structural model.

Nominal composition x/y	$In_{2.67}S_{4-x}Se_x$				$In_{2.67}S_{4-y}Te_y$		
	0.1	0.15	0.2	0.5	0.05	0.1	0.15
Type of refinement	two-phase					single-phase	
Space group, Pearson symbol, no. of formula units Z	$Fd\bar{3}m$, $cF56$, 8						
a [Å] ^{a)}	10.7869(2)	10.7891(1)	10.7950(2)	10.8232(2)	10.7879(2)	10.7998(2)	10.8111(1)
V [Å ³] ^{a)}	1255.1(1)	1255.9(1)	1258.0(1)	1267.8(1)	1255.5(1)	1259.6(1)	1263.6(1)
d_{XRD} [g·cm ⁻³] ^{b)}	4.6479(3)	4.6697(3)	4.6867(3)	4.7979(3)	4.6473(3)	4.6826(3)	4.7180(3)
λ [Å]	1.54056						
$2\theta_{max}$ [°]; $\sin\theta/\lambda$ (max)	100.30; 0.498						
No. of refined reflections	46						
Phase fraction [%]	69	-					
R_I , $R_{P,CSD}$, $R_{WP,CSD}$ [%]	3.43, 14.08, 14.84	3.07, 9.76, 11.39	2.79, 9.62, 10.73	2.81, 8.94, 10.06	3.41, 7.96, 7.78	3.37, 8.98, 8.76	4.46, 11.32, 11.51
R_P , R_{WP} [%]	5.51, 7.97	4.23, 6.21	3.97, 5.84	3.70, 5.50	2.84, 4.24	3.02, 4.44	3.82, 5.69
In1 at $8a$ ($^{1/8} \text{ } ^{1/8} \text{ } ^{1/8}$), B_{iso} [Å ²]	1.71(3)	0.8(3)	0.7(3)	0.7(3)	1.3(2)	1.4(3)	1.4(3)
In2 at $16d$ ($^{1/4} \text{ } ^{0} \text{ } ^{3/4}$), B_{iso} [Å ²]	2.05(3)	1.1 (1)	1.1(1)	1.2(1)	1.8(1)	1.6(1)	1.7(2)
S/Se/Te at $32e$ ($u \text{ } u \text{ } u$), u / B_{iso} [Å ²]	2541(9 / 1.20(1))	0.2566(8) / 0.8(4)	0.2566(8) / 0.7(4)	0.2561(6) / 0.7(3)	0.2540(7) / 1.4(2)	0.2545(8) / 1.7(4)	0.2537(10) / 1.9(4)
SOF(In at $8a$) ^{c)}	0.67	0.68(2)	0.67(2)	0.67(2)	0.66(2)	0.69(2)	0.69(2)
Fraction of Se/Te at $32e$	-	0.05(3)	0.05(3)	0.13(3)	0	0.03(1)	0.05(3)
$4 \times In1$ -S [Å]	-	2.458(8)	2.459(9)	2.456(7)	2.410(8)	2.421(8)	2.41(1)
$6 \times In2$ -S [Å]	-	2.627(8)	2.629(9)	2.641(7)	2.654(8)	2.651(8)	2.66(1)
S-S [Å]	-	3.61(1)	3.62(1)	3.640(9)	3.69(1)	3.68(1)	3.71(1)

a) Given unit-cell parameters were refined separately with LaB₆ as an internal standard (values are also shown in the Figure 2). b) Densities were calculated for nominal chemical compositions. c) SOF – site occupancy factor.

WinCSD software provides two sets of reliability factors: (i) profile $R_{P,CSD}$ and weighted-profile $R_{WP,CSD}$, which are calculated with background subtraction, and (ii) profile R_P and weighted-profile R_{WP} , which are calculated without background subtraction.¹ Therefore, larger values are observed for the set (i). All these parameters are defined as follows:

$$\begin{aligned}
 R_I &= \frac{\sum_k |I_{obs,k} - I_{calc,k}|}{\sum_k I_{obs,k}} \\
 R_{P,CSD} &= \frac{\sum_k |(y_{obs,k} - bg_{obs,k}) - (y_{calc,k} - bg_{calc,k})|}{\sum_k (y_{obs,k} - bg_{obs,k})} \\
 R_{WP,CSD} &= \frac{\sum_k w_k [(y_{obs,k} - bg_{obs,k}) - (y_{calc,k} - bg_{calc,k})]^2}{\sum_k w_k (y_{obs,k} - bg_{obs,k})^2}
 \end{aligned}$$

$$R_P = \frac{\sum_k |y_{obs,k} - y_{calc,k}|}{\sum_k y_{obs,k}}$$

$$R_{WP} = \left(\frac{\sum_k w_k (y_{obs,k} - y_{calc,k})^2}{\sum_k w_k y_{obs,k}^2} \right)^{\frac{1}{2}}$$

$$w_k = \frac{1}{\sigma^2(y_{obs,k})}$$

where: I_k is integrated intensity of the k -th peak, whereas y_k , bg_k , w_k and $\sigma(y_k)$ denote intensity, background values, weight and standard uncertainty, respectively, at the k -th data point.

Table S3. Density after SPS d_{SPS} compared with crystallographic density d_{XRD} from Rietveld refinement.

Series	x/y	d_{XRD} [g·cm ⁻³]	d_{SPS} [g·cm ⁻³]	$d_{SPS}/d_{XRD} \times 100\%$
$In_{2.67}S_{4-x}Se_x$	0	4.6137(3)	4.575(4)	99.1
	0.1	4.6480(3)	4.625(3)	99.5
	0.15	4.6697(3)	4.629(3)	99.1
	0.2	4.6867(3)	4.666(1)	99.6
	0.5	4.7979(3)	4.767(7)	99.4
$In_{2.67}S_{4-y}Te_y$	0.05	4.6473(3)	4.625(3)	99.5
	0.1	4.6826(3)	4.673(5)	99.8
	0.15	4.7180(3)	4.703(4)	99.7

2. Raman spectroscopy

Table S4. List of all observed Raman modes [cm⁻¹] for In_{2.67}S_{4-x}Se_x and In_{2.67}S_{4-y}Te_y compounds. Broad bands composed of multiple peaks are listed as ranges. Modes presented in ()-brackets were detected only for some grains. Fingerprints of tetragonal β -In_{2.67}S₄ are highlighted in blue.

Se-series, x					Te-series, y			Literature: β -In _{2.67} S ₄	
0	0.1	0.15	0.2	0.5	0.05	0.1	0.15	Kambas <i>et al.</i> ²	Wyżga <i>et al.</i> ³
62	~63	64	65	64	66	65	65	61	64
72	(68)	70	~76		(69)			70	73
83									85
90	89	90							91
101	101	~101	~101	~100		104		102	102
115	(113)	114			(113)			113	116
121									122
135	(~135)	135			(~135)	(~131)		137	137
~170					(~171, 176)	~171	173		171
180	145– 220	~180		148– 225				180	181
195		~195	~197					196	198
215								217	219
245	246	245	248	255	244– 249	249	351	244	246
265	~265	264	267		(~260)			266	267
307	305	306	304	301	304	304	302	306	309
326		323		~328				326	327
367	362	364	356	355	360– 361	358	350	367	369

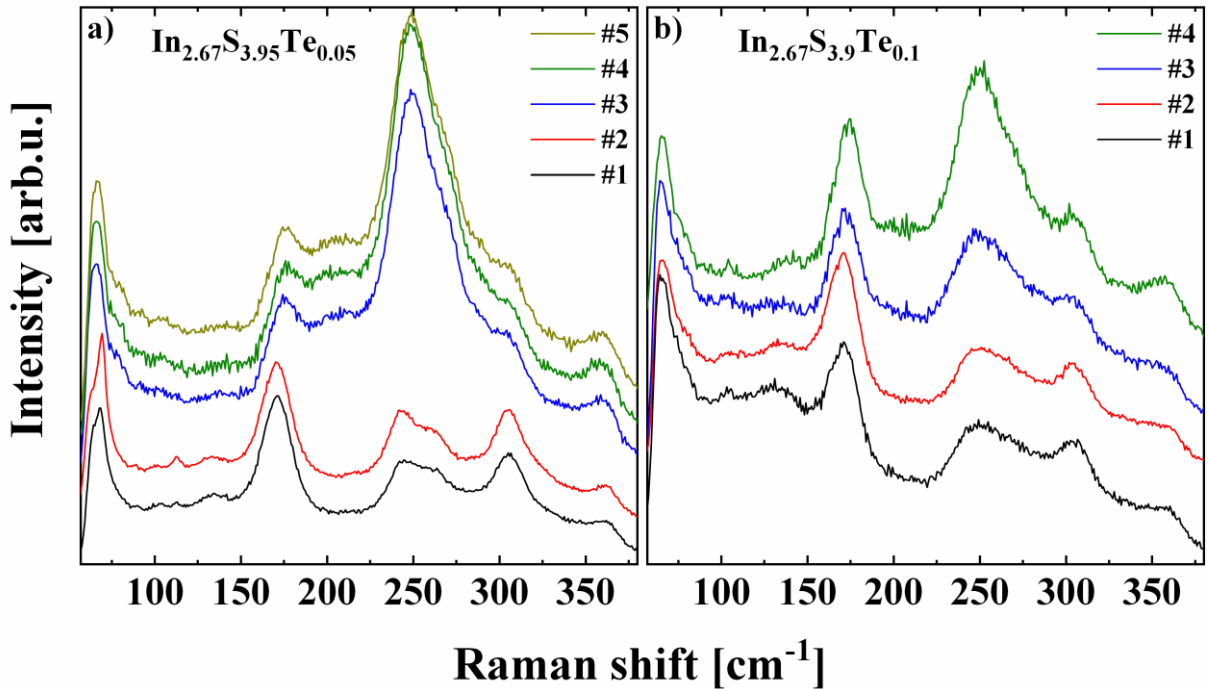


Figure S3. Raman spectra of a) In_{2.67}S_{3.95}Te_{0.05} and b) In_{2.67}S_{3.9}Te_{0.1} samples. Peak intensities are scaled according to modes at ~ 170 cm⁻¹. Labels #1–#5 indicate different spots on the samples.

3. Thermal analysis

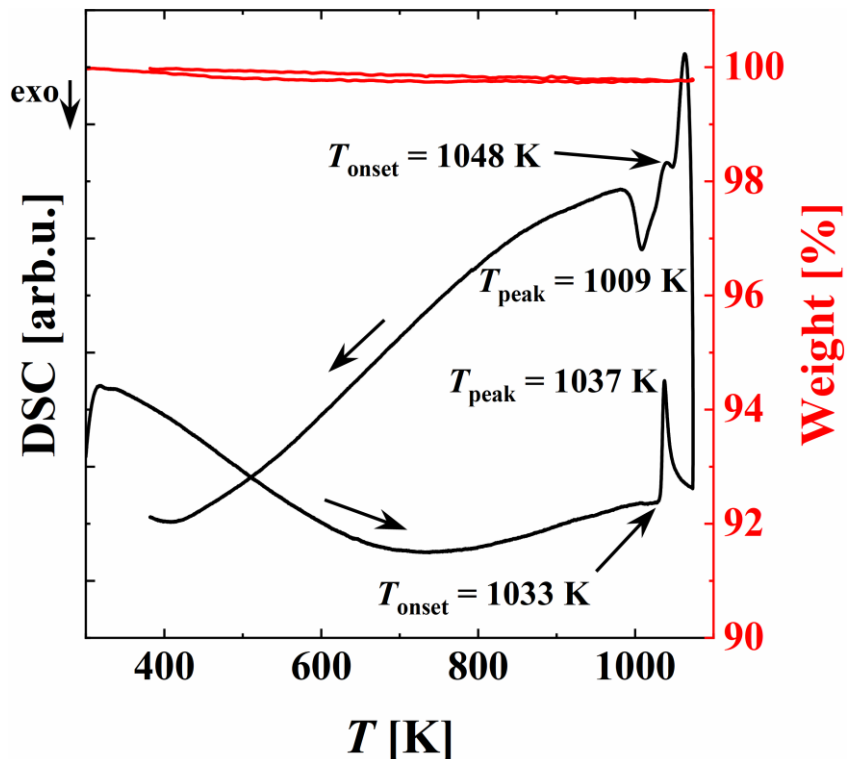


Figure S4. Differential scanning calorimetry and thermogravimetry simultaneously measured for the $\text{In}_{2.67}\text{S}_{3.9}\text{Se}_{0.1}$ sample with heating/cooling rate of $10 \text{ K} \cdot \text{min}^{-1}$.

The observed reversible thermal effect (endothermic upon heating) is connected with the α - γ phase transition of indium thiospinel.⁴ The mass loss was smaller than 0.3 wt.%.

4. Density functional theory calculations

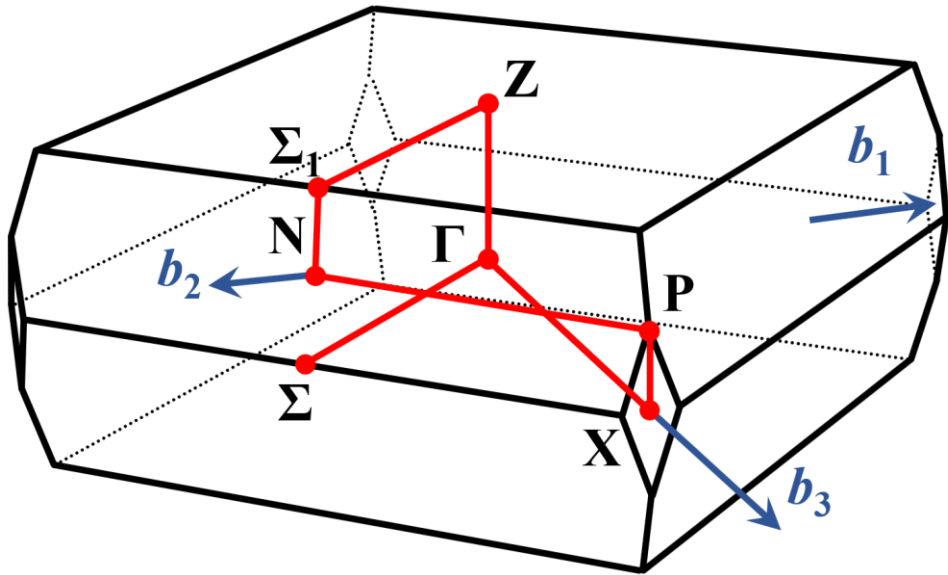


Figure S5. The 1st Brillouin zone for *I4₁/amd* space group with the ratio $c_{\text{tetr}}/a_{\text{tetr}} = 4.24$. b_1 , b_2 and b_3 denote primitive reciprocal lattice vectors. The electronic band structures were calculated between special points along the path: Σ - Γ - X - P - N - Σ_1 - Z - Γ . Coordinates of points in the primitive cell: $\Gamma(0, 0, 0)$, $\Sigma(-\eta, \eta, \eta)$, $X(0, 0, \frac{1}{2})$, $P(\frac{1}{4}, \frac{1}{4}, \frac{1}{4})$, $N(0, \frac{1}{2}, 0)$, $\Sigma_1(\frac{1}{2}-\eta, \frac{1}{2}+\eta, \eta^{-\frac{1}{2}})$, $Z(\frac{1}{2}, \frac{1}{2}, -\frac{1}{2})$ where $\eta = (1+a^2/c^2)/4$.⁵ Points Σ and Σ_1 are symmetrically equivalent.⁶

5. Single parabolic band model

According to Boltzmann transport theory,⁷ following parameters are obtained in the function of the reduced Fermi energy η :

Seebeck coefficient

$$\alpha(\eta) = \frac{k}{e} \left[\frac{(r + 5/2)F_{(r+3/2)}(\eta)}{(r + 3/2)F_{(r+1/2)}(\eta)} - \eta \right]$$

Charge carrier concentration
(from Hall measurement)

$$n_H = \frac{1}{eR_H}$$

Effective electron mass

$$m_e^*(\eta) = \frac{1}{2kT} \left(3\pi^2 \hbar^3 n_H(\eta) \frac{(2r + 3/2)F_{(2r+1/2)}(\eta)}{(r + 3/2)^2 F_{(r+1/2)}^2(\eta)} \right)^{2/3}$$

Lorenz number

$$L(\eta) = \left(\frac{k}{e} \right)^2 \left\{ \frac{(r + 7/2)F_{(r+5/2)}(\eta)}{(r + 3/2)F_{(r+1/2)}(\eta)} - \left[\frac{(r + 5/2)F_{(r+3/2)}(\eta)}{(r + 3/2)F_{(r+1/2)}(\eta)} \right]^2 \right\}$$

Fermi integral

$$F_j(\eta) = \int_0^\infty \frac{E^j}{1 + e^{(E-\eta)}} dE$$

For ionized impurity scattering (IIS) scattering factor $r = 1.5$, whereas for acoustic phonon scattering (APS) $r = -0.5$.

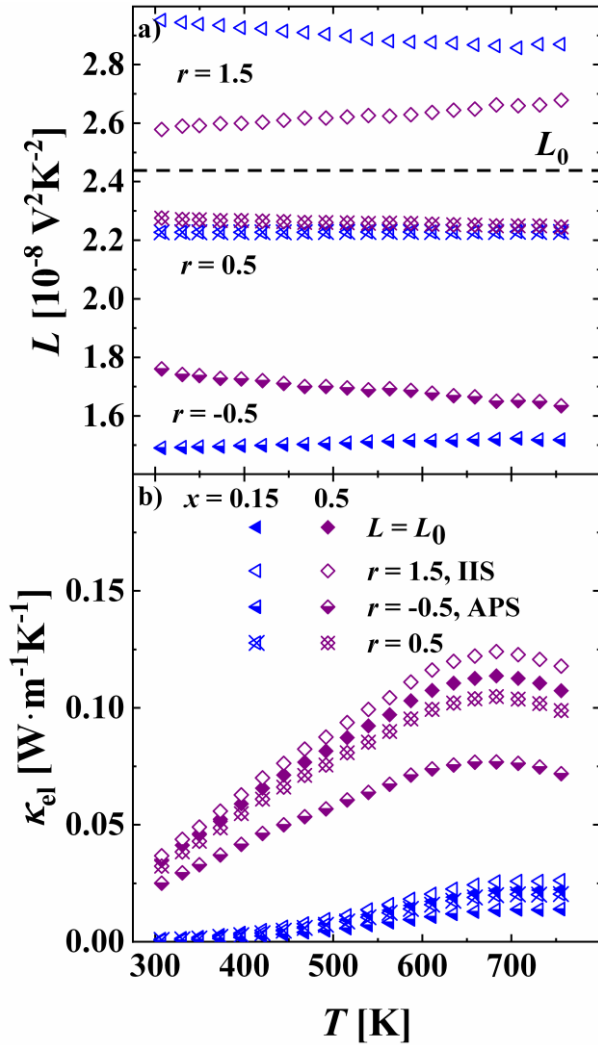


Figure S6. Comparison of a) Lorenz numbers and b) electronic thermal conductivities calculated for the selected $\text{In}_{2.67}\text{S}_{4-x}\text{Se}_x$ samples assuming different scattering factors r . $L_0 = 2.44 \times 10^{-8} \text{ V}^2 \text{ K}^{-2}$. IIS - ionized impurity scattering. APS - acoustic phonon scattering.

The comparison of experimentally and theoretically determined effective electron masses (from SPB model and DFT calculations, respectively) suggests that at least two different scattering mechanisms contribute to the electrical transport in the studied compounds. Moreover, the previous reports on the binary and ternary indium thiospinels revealed that IIS is a dominating contribution.^{3,8} Since we do not know T -dependence of mobility for the Se/Te-substituted compounds, there is also no information about scattering factors r . If one would assume $0.5 \leq r \leq 1.5$ (which seems to be a realistic range for the studied here thiospinels), extremal Lorenz values L (*i.e.*, for $r = -0.5$ and 1.5) would differ by less than 33 % for high-resistivity samples (*e.g.*, $\text{In}_{2.67}\text{S}_{3.85}\text{Se}_{0.15}$) and less than 20 % for low-resistivity (*e.g.*, $\text{In}_{2.67}\text{S}_{3.5}\text{Se}_{0.5}$)

samples, whereas L_0 would lie within this range (Figure S6a). Nevertheless, differences between absolute κ_{el} -values remain insignificant (Figure S6b). Therefore, we assumed constant Lorenz number $L = L_0$ in the Wiedemann-Franz law calculations.

References

1. L. Akselrud and Y. Grin, *J. Appl. Crystallogr.*, 2014, **47**, 803–805.
2. K. Kambas, J. Spyridelis and M. Balkanski, *Phys. Status Solidi*, 1981, **105**, 291–296.
3. P. Wyżga, I. Veremchuk, C. Himcinschi, U. Burkhardt, W. Carrillo-Cabrera, M. Bobnar, C. Hennig, A. Leithe-Jasper, J. Kortus and R. Gumeniuk, *Dalton Trans.*, 2019, **48**, 8350–8360.
4. T. Gödecke and K. Schubert, *Z. Metallkd.*, 1985, **76**, 358–364.
5. W. Setyawan and S. Curtarolo, *Comput. Mater. Sci.*, 2010, **49**, 299–312.
6. U. Shmueli, Ed., *International Tables for Crystallography. Volume B*, Kluwer Academic Publishers, 2nd edn., 2001.
7. H. J. Goldsmid, *Introduction to Thermoelectricity*; Springer-Verlag Berlin Heidelberg, **2010**.
8. P. Wyżga, I. Veremchuk, M. Bobnar, P. Koželj, S. Klenner, R. Pöttgen, A. Leithe-Jasper and R. Gumeniuk, *Chem. Eur. J.*, 2020, **26**, 5245–5256.